IEEE Photonics Journal
An IEEE Photonics Society Publication

Open Access

Light Extraction Efficiency Analysis of Flip-Chip Ultraviolet Light-Emitting Diodes With Patterned Sapphire Substrate

Volume 10, Number 4, August 2018

Yu Kee Ooi
Jing Zhang

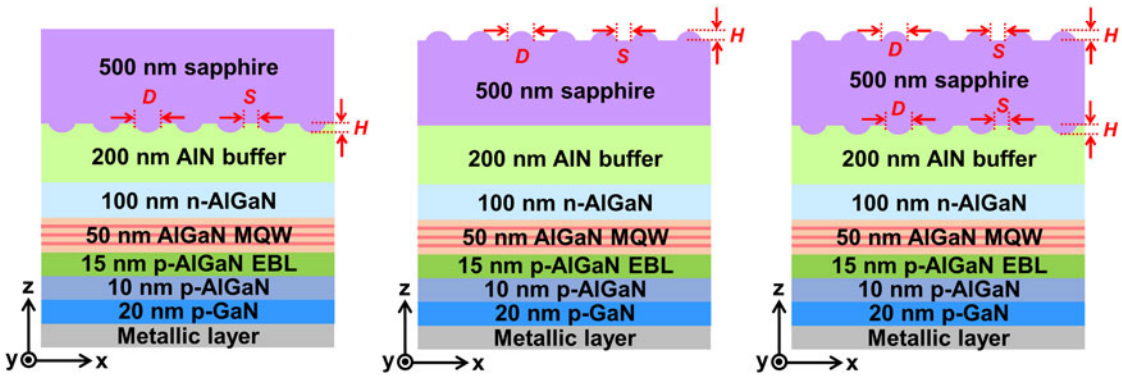

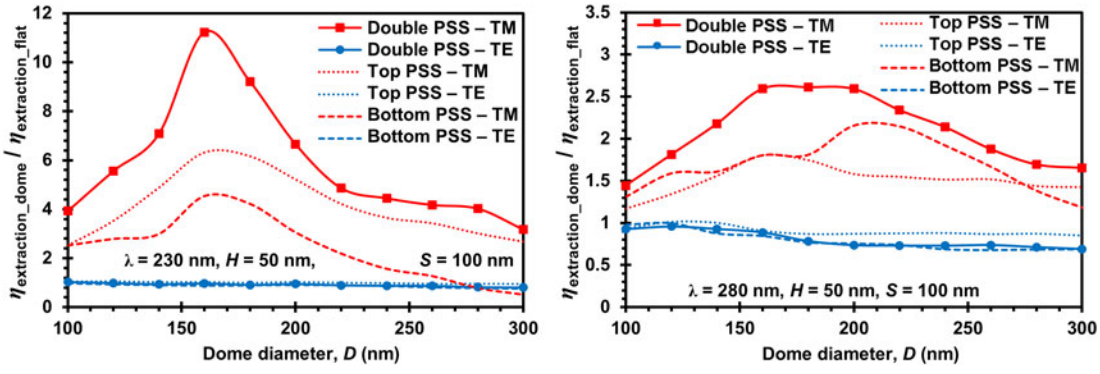

DOI: 10.1109/JPHOT.2018.2847226

Light Extraction Efficiency Analysis of Flip-Chip Ultraviolet Light-Emitting Diodes With Patterned Sapphire Substrate

Yu Kee Ooi [1] **and Jing Zhang** [1,2]

[1]Microsystems Engineering, Rochester Institute of Technology, Rochester, NY 14623 USA
[2]Department of Electrical and Microelectronic Engineering, Rochester Institute of Technology, Rochester, NY 14623 USA

DOI:10.1109/JPHOT.2018.2847226

Manuscript received June 1, 2018; accepted June 8, 2018. Date of publication June 13, 2018; date of current version July 16, 2018. This work was supported in part by the Rochester Institute of Technology Kate Gleason endowed professorship fund, in part by the Office of Naval Research under Grant N00014-16-1-2524, and in part by the National Science Foundation under Grant 1751675. Corresponding authors: Yu Kee Ooi and Jing Zhang (email: Yu.Kee.Ooi@rit.edu; Jing.Zhang@rit.edu).
This paper has supplementary downloadable material available at http://ieeexplore.ieee.org.

Abstract: This study investigates polarization-dependent light extraction efficiency ($\eta_{extraction}$) of AlGaN-based flip-chip ultraviolet (UV) light-emitting diodes (LEDs) emitting at 230 nm and 280 nm with microdome-shaped patterning on sapphire substrate based on 3-D finite-difference time-domain simulations. Three types of patterned sapphire substrates (PSS) have been analyzed: bottom-side PSS, top-side PSS, and double-sided PSS. Our results show that microdome-shaped patterning on sapphire substrate is predominantly beneficial in enhancing transverse-magnetic (TM)-polarized output. Specifically, TM-polarized $\eta_{extraction}$ enhancement of up to ~4.5 times and ~2.2 times can be obtained for 230 nm and 280 nm UV LEDs with bottom-side PSS, respectively, and ~6.3 times and ~1.8 times for 230 nm and 280 nm UV LEDs with top-side PSS, respectively. By employing double-sided PSS, up to ~11.2 times and ~2.6 times enhancement in TM-polarized $\eta_{extraction}$ can be achieved for 230 nm and 280 nm UV LEDs, respectively. In contrast, the microdome-shaped PSS act as a reflector for transverse-electric-polarized photons which leads to severe limitation in light extraction for both 230 nm and 280 nm flip-chip UV LEDs. Thus, it is expected that this study will serve as a guidance in designing PSS for high-efficiency mid- and deep-UV LEDs.

Index Terms: Patterned sapphire substrate, polarization-dependent light extraction efficiency, quantum well structure, ultraviolet light-emitting diodes.

1. Introduction

III-nitride-based optoelectronic devices have been employed extensively in wide variety of applications attributed to their compact sizes, higher energy efficiency, longer lifetime and robustness. As a result, ternary AlGaN alloys have been considered as promising candidates in replacing conventional ultraviolet (UV) light sources for applications such as photolithography, resin curing for three-dimensional (3D) printing, water and air purification, sterilization, and bioagent detection [1]–[4]. Nevertheless, the growth challenges for high-quality Al-rich AlGaN epilayers have impeded the realization of high efficiency UV light-emitting diodes (LEDs) as the difficulties in p-type doping for AlGaN layer has limited the injection efficiency ($\eta_{injection}$) [5], [6] while the large threading dislocation density from AlGaN materials has resulted in low internal quantum efficiency (η_{IQE}) [7],

[8]. Additionally, strong UV light absorption in p-GaN contact layer as well as anisotropic emission at high Al-composition AlGaN quantum wells (QWs) in deep-UV regime [9]–[12] have restricted the light extraction efficiency ($\eta_{extraction}$) from AlGaN-based planar UV LEDs. Consequently, <10% of external quantum efficiency (η_{EQE}) has been reported for planar AlGaN-based QW UV LEDs with emission wavelength (λ) < 300 nm, and the η_{EQE} further drops to ~1% for $\lambda < 250$ nm [3], [13], [14]. Various fabrication methods and growth techniques have been proposed to address issues associated with low $\eta_{injection}$ and η_{IQE} [15]–[29]. On the other hand, various LED device structures such as flip-chip design [30], [31], patterned sapphire substrate (PSS) [14], [20], [32], patterned p-type layer [33], and nanowire structure [34]–[36] have been investigated for enhancing the $\eta_{extraction}$ of UV LEDs.

Among all the proposed methods for improving the $\eta_{extraction}$, the use of PSS has received significant attention due to 1) reduced fabrication complexities, and 2) minimized dislocation density from epitaxial growths, which reduces the possibility of photons trapping in the defect sites [20], [32]. Recent experimental work on 282 nm AlGaN-based UV LEDs with nano-PSS has reported 3.45% of η_{EQE} (~98% enhancement as compared to LED with flat sapphire surface) [20], while experimental study on 275 nm flip-chip LEDs with PSS has recorded maximum $\eta_{EQE} > 16\%$ (~4-times larger than flip-chip LED with flat sapphire substrate) [14]. In spite of these encouraging experimental results, there has been very limited works exploring the polarization-dependent $\eta_{extraction}$ for flip-chip UV LEDs with PSS, which is particularly important for AlGaN-based UV LEDs as emission from AlGaN QW with $\lambda < 230$–240 nm is primarily transverse-magnetic (TM) [$\boldsymbol{E}$ // c-axis] dominant whereas $\lambda > 250$ nm is mostly transverse-electric (TE) [$\boldsymbol{E} \perp$ c-axis] dominant [9], [10].

In this work, we examined the light extraction mechanisms for flip-chip UV LEDs with microdome-shaped array patterning on sapphire substrate based on 3D finite-difference time-domain (FDTD) method. The patterning of sapphire substrate on the bottom-side (the epitaxial growth side) has been commonly used in experimental work to minimize dislocation density [20], [32] but very limited work has been devoted to investigate the effect of PSS on the $\eta_{extraction}$, particularly the top-side and double-sided patterning on the sapphire substrate. Therefore, in particular, we study the polarization dependence $\eta_{extraction}$ of 230 nm (typically TM-dominant emission peak [9], [34]) and 280 nm (typically TE-dominant emission peak [9]) AlGaN-based flip-chip UV LEDs with microdome-shaped array patterning on bottom-side, top-side and double-sided of sapphire substrates arranged in hexagonal pattern.

2. 3D FDTD Simulation Method

In this study, the $\eta_{extraction}$ for AlGaN-based multiple QW (MQW) flip-chip UV LEDs emit at 230 nm and 280 nm with microdome-shaped array patterning on sapphire substrate have been investigated using 3D FDTD method [37], which is commonly used in analyzing the optical properties of III-nitride emitters [30], [31], [33]–[36], [38]. The layer structure of the UV LEDs used in the simulations are illustrated in Fig. 1 which consist of 500 nm thick sapphire substrate, 200 nm AlN buffer layer, 100 nm n-AlGaN layer, 50 nm thick AlGaN layer to represent the MQW active region, 15 nm p-AlGaN electron blocking layer (EBL), 10 nm p-AlGaN layer and 20 nm p-GaN contact layer. A metallic layer that acts as a perfect mirror is attached to the bottom of the LED to reflect all photons incident upon it. Fig. 1(a) shows the UV LED with microdome-shaped array patterning on the bottom surface of sapphire substrate, Fig. 1(b) shows the UV LED with microdome-shaped array patterning on the top surface of sapphire substrate, and Fig. 1(c) shows the UV LED with microdome-shaped array patterning on both sides of sapphire substrate. The microdome patterning with diameter, D, height, H, and spacing, S, are arranged in hexagonal pattern on sapphire substrate, as depicted in Fig. 1(d). Since this work focuses on comparing the $\eta_{extraction}$ for UV LEDs with various position of microdome-shaped array on sapphire substrate, only D is set as variable in the study while H and S are fixed at 50 nm and 100 nm respectively. The values for H and S are determined from our internal comprehensive analysis where the TM-polarized $\eta_{extraction}$ drops substantially to < 10% when $S > 100$ nm while larger H will result in significantly improved $\eta_{extraction}$. However, considering the practicality

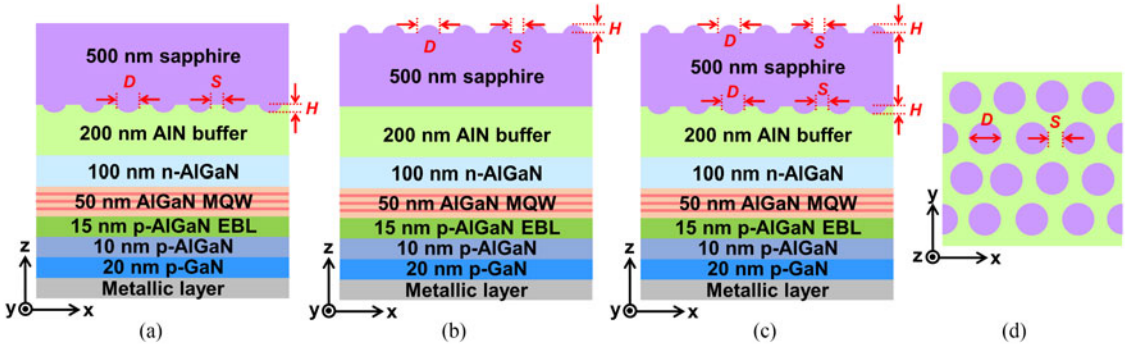

Fig. 1. Schematic side view of AlGaN-based flip-chip UV LED with microdome-shaped array patterning on (a) bottom-side, (b) top-side and (c) double-sided of sapphire substrate. The diameter, spacing and height of the microdomes are labeled as *D*, *S*, and *H* respectively. (d) Top view showing the microdome-shaped array on sapphire substrate arranged in hexagonal pattern.

and complexity in forming taller microdomes on sapphire substrate during the fabrication process, $H = 50$ nm is chosen in this study.

The refractive indexes and absorption coefficients for AlN, GaN and sapphire are taken from [30], [39], [40]. Linear extrapolation between AlN and GaN is used in calculating the refractive indexes and absorption coefficients for ternary AlGaN layers where the Al-content for the corresponding emission wavelength are determined from [41]. To be more specific, the Al composition for 230 nm emission wavelength is deduced as 98% for p-AlGaN EBL, 77% for AlGaN MQW, and 86% for both the n- and p-AlGaN, while for 280 nm emission wavelength is deduced as 93% for p-AlGaN EBL, 42% for AlGaN MQW, and 64% for both the n- and p-AlGaN. As 3D FDTD simulation consumes a large amount of memory and computation time, the simulation domain is set to 5 μm $\times$ 5 μm in the lateral direction in order to ensure computation efficiency. Non-uniform grid size of 10 nm in the bulk and 5 nm near the edges is used in the simulation. Perfectly matched layer boundary condition is applied to the lateral and top boundaries while perfect electric conductor boundary condition is applied to the bottom boundary. A single dipole source is placed at the center of the AlGaN MQW active region where TE-polarization is defined as the major electric field travels in the in-plane direction (parallel to the *x* and *y* directions labeled in Fig. 1) while TM-polarization is represented by the major electric field travels in the out-of-plane direction (parallel to the *z* direction labeled in Fig. 1). Single dipole source is used in this work as the use of multiple dipole sources will result in non-physical interference pattern [42], which is undesirable for analysis of the optical properties of LEDs. A source power monitor surrounding the dipole source is used to measure the total power generated in the active region while one output power monitor is placed at distance λ away from the sapphire top surface to measure the light output power radiated out of the LED structure. The $\eta_{extraction}$ is calculated as ratio of the light output power measured by the output power monitor to the total power dissipated by the dipole source in the active region [30], [38].

3. Results and Discussion

3.1 Flip-Chip UV LEDs With Flat Sapphire Substrate

The flip-chip UV LED with flat sapphire substrate has first been investigated as a reference in this work. For 280 nm UV LED, the calculated TM- and TE-polarized $\eta_{extraction}$ is ~0.74% and ~13% respectively. As spontaneous emission from 280 nm AlGaN QW is largely TE-polarized [34], high η_{EQE} is expected from the 280 nm flip-chip UV LEDs with flat sapphire substrate. Thus, the study on the effect of PSS to the polarization-dependent $\eta_{extraction}$ for 280 nm flip-chip UV LEDs is essential to further enhance the η_{EQE} and for realizing high efficiency mid-UV LEDs.

On the other hand, for 230 nm UV LED, the calculated TM-polarized $\eta_{extraction}$ is ~0.13% while the calculated TE-polarized $\eta_{extraction}$ is ~13%. Although significantly larger TE-polarized $\eta_{extraction}$ can

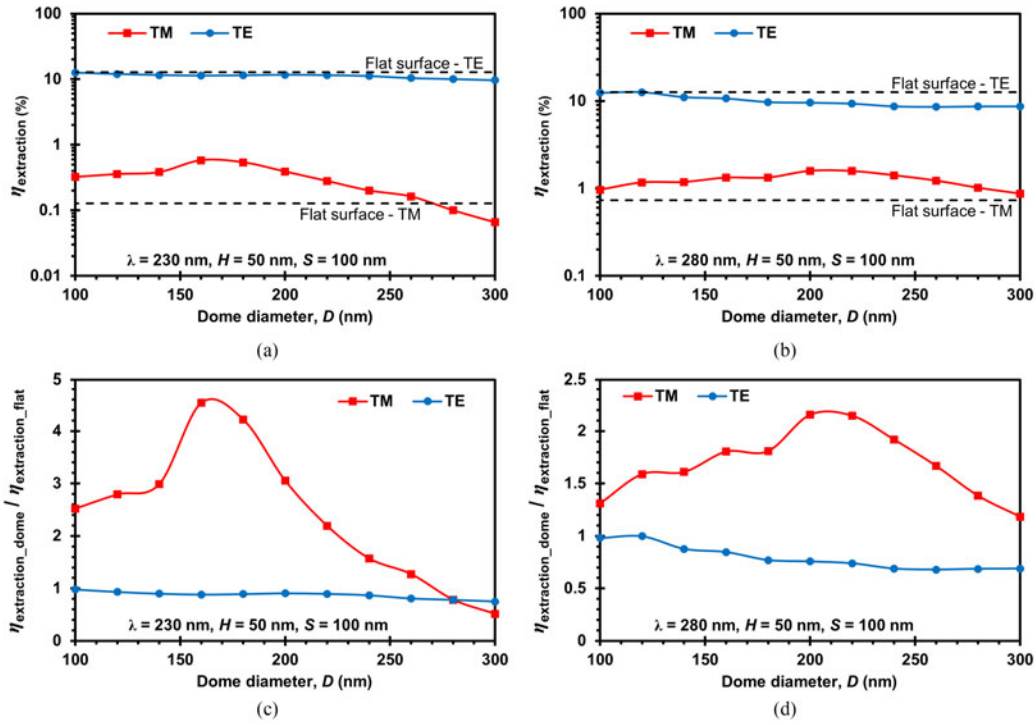

Fig. 2. The $\eta_{extraction}$ for AlGaN-based flip-chip UV LEDs with bottom side PSS at (a) $\lambda = 230$ nm and (b) $\lambda = 280$ nm as a function of D. The $\eta_{extraction}$ for UV LEDs with flat sapphire substrate are represented by the black dashed lines. Ratio of the $\eta_{extraction}$ for UV LEDs with bottom-side PSS ($\eta_{extraction\_dome}$) to the $\eta_{extraction}$ for flip-chip UV LEDs with flat sapphire substrate ($\eta_{extraction\_flat}$) for (c) $\lambda = 230$ nm and (d) $\lambda = 280$ nm as a function of D.

be obtained from planar UV LED with flat sapphire substrate, the TM-polarized output at 230 nm is ~20-times higher than the TE-polarized output [34]. As TM-polarized light is primarily propagates in the lateral direction, very limited amount of photons can be extracted from the top and bottom sides of the device, which results in extremely low TM-polarized $\eta_{extraction}$. Consequently, it is very challenging to achieve high η_{EQE} for conventional planar structure 230 nm UV LEDs. Therefore, it is strongly motivated to investigate the polarization-dependent $\eta_{extraction}$ of 230 nm flip-chip UV LEDs with PSS in order to further improve the TM-polarized $\eta_{extraction}$.

3.2 Flip-Chip UV LEDs With Microdome-Shaped Patterning on Bottom Side of Sapphire Substrate

The $\eta_{extraction}$ for flip-chip UV LEDs with microdome-shaped array on the bottom surface of sapphire substrate is plotted in Fig. 2 as a function of D. Figs. 2(a) and 2(b) present the $\eta_{extraction}$ of flip-chip UV LEDs with microdome-shaped patterning on bottom surface of sapphire substrate for 230 nm and 280 nm respectively. The $\eta_{extraction}$ for conventional flip-chip UV LEDs with flat sapphire substrate is also plotted for comparison purpose. As illustrated in Figs. 2(a) and 2(b), the TE-polarized $\eta_{extraction}$ for both 230 nm and 280 nm are consistently higher than TM-polarized $\eta_{extraction}$ (>1 order of magnitude) when D changes from 100 nm to 300 nm. For instance, the ratios between TE and TM polarizations are observed as ~40-times and ~13-times for 230 nm and 280 nm UV LEDs respectively when $D = 100$ nm, and ~20-times and 8-times for 230 nm and 280 nm UV LEDs respectively when $D = 160$ nm. Since TM-polarized light tends to emit at large angles with respect to c-axis (parallel to the z direction labeled in Fig. 1) while planar LED structure favors light extraction along c-axis, majority of the TM-polarized output is trapped inside the LED structure which results in lower TM-polarized $\eta_{extraction}$ as compared to TE-polarized $\eta_{extraction}$ for both emission wavelengths.

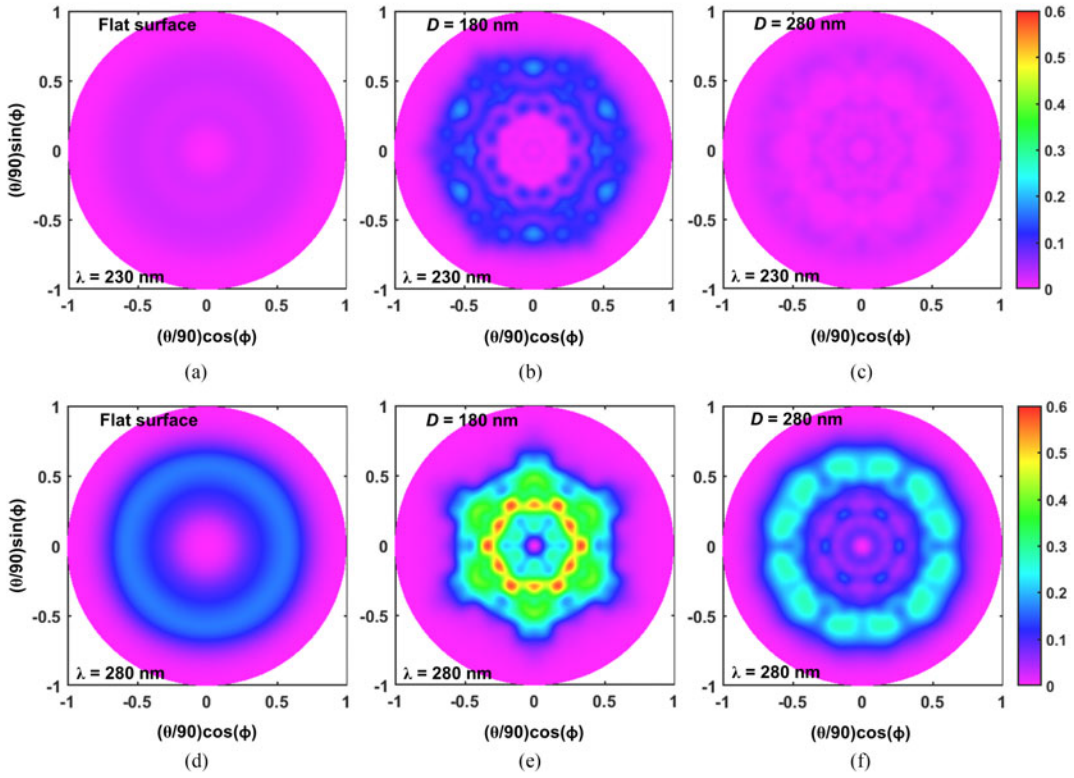

Fig. 3. TM-polarization far-field radiation patterns of 230 nm [(a)–(c)] and 280 nm [(d)–(f)] flip-chip UV LEDs with flat sapphire substrate [(a) & (d)], bottom-side PSS with $D = 180$ nm [(b) & (e)] and bottom-side PSS with $D = 280$ nm [(c) & (f)].

Despite lower TM-polarized $\eta_{extraction}$ than TE-polarized $\eta_{extraction}$ is observed, the TM-polarized $\eta_{extraction}$ for both 230 nm and 280 nm UV LEDs with bottom-side PSS demonstrate strong dependence on the microdome diameter as D changes from 100 nm to 300 nm. The use of PSS could act as extractor or reflector, depending on the ratio of light being scattered out of the structure to light being scattered back into the structure. When the fraction of light being scattered out of the structure is larger than the fraction of light being scattered back into the structure, the PSS serves as an extractor which could lead to enhanced $\eta_{extraction}$. Otherwise, the PSS will serve as a reflector that inhibit light extraction through the sapphire substrate. From the results presented in Fig. 2, the microdome-shaped array on the bottom side of sapphire substrate with $D < 280$ nm acting more like an extractor for TM-polarized photons but as a reflector for TE-polarized photons. This is evidenced in the cross-sectional near-field electric field intensity plots shown in Figs. S1(b), S1(c), S1(i) & S1(j) for TM-polarization and Figs. S2(b), S2(c), S2(i) & S2(j) for TE-polarization in the supplementary information. As shown in Figs. 2(c) and 2(d), up to ~4.5-times and ~2.2-times enhancement in TM-polarized $\eta_{extraction}$ can be obtained for 230 nm and 280 nm UV LEDs with bottom-side PSS respectively whereas lower TE-polarized $\eta_{extraction}$ for UV LEDs with bottom-side PSS than with flat sapphire substrate are observed for both 230 nm and 280 nm when D changes from 100 nm to 300 nm. Specifically, for TM-polarization, the peak $\eta_{extraction}$ enhancement is observed when D is ~70–80 nm below the emission wavelength for UV LEDs with bottom-side PSS.

As described previously, the use of PSS enhances the scattering of photons which results in modified light radiation pattern and the $\eta_{extraction}$. For conventional UV LEDs with flat sapphire substrate, both the 230 nm and 280 nm devices exhibit symmetric donut-shaped radiation patterns with peak intensity at ~30° with respect to c-axis [Figs. 3(a) and 3(d)]. Lower intensity is observed for 230 nm UV LED as compared to 280 nm UV LED due to the larger refractive index contrast between the AlGaN/GaN layers, sapphire and air medium for 230 nm. For both emission wavelengths, when

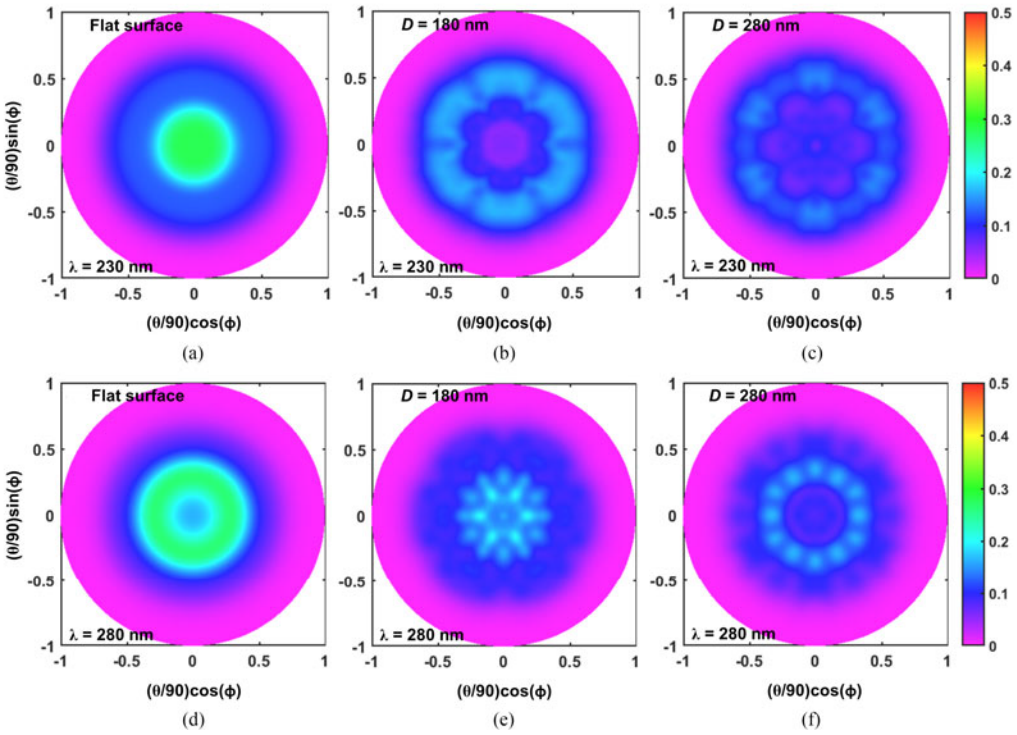

Fig. 4. TE-polarization far-field radiation patterns of 230 nm [(a)–(c)] and 280 nm [(d)–(f)] flip-chip UV LEDs with flat sapphire substrate [(a) & (d)], bottom-side PSS with $D = 180$ nm [(b) & (e)] and bottom-side PSS with $D = 280$ nm [(c) & (f)].

$D = 180$ nm, UV LEDs with bottom-side PSS show higher radiation intensity over large angle range (~25° to ~40° for 230 nm and ~10° to ~40° for 280 nm) [Figs. 3(b) and 3(e)]. In addition, overall higher radiation intensity is also observed attributed to the curvature surfaces of the microdomes that result in larger photon escape cone as compared to conventional UV LEDs. This spread-out distribution of high intensity radiation pattern for the investigated UV LEDs with bottom-side PSS has contributed to the larger TM-polarized $\eta_{extraction}$ (~4.2-times and 1.8-times for 230 nm and 280 nm respectively) than the conventional UV LEDs with flat sapphire substrate.

For the case of $D = 280$ nm, the bottom-side PSS is suppressing the extraction of 230 nm TM-polarized photons [Fig. 3(c)], which results in lower $\eta_{extraction}$ (~0.8-times) than the UV LEDs with flat sapphire substrate. However, substantial improvement in the TM-polarized $\eta_{extraction}$ (~1.4-times) for 280 nm UV LEDs can still be obtained attributed to the high radiation intensity at angles between 20° and 40° [Fig. 3(f)]. These results suggest that the optimum microdome design on the bottom side of sapphire substrate is smaller D than the UV LED emission wavelength, preferably ~70–80 nm below the emission wavelength. Microdomes with large D should be avoided to prevent the bottom-side microdome-shaped PSS to act as reflector that limit the extraction of TM-polarized light through the sapphire substrate, as evidenced by the cases of $D > 260$ nm for 230 nm UV LEDs.

As opposed to TM-polarization, the bottom-side PSS acts as reflector that inhibit TE-polarized light extraction through the sapphire substrate. As illustrated in Fig. 4, significantly lower radiation intensity for both 230 nm and 280 nm UV LEDs with bottom-side microdome-shaped PSS is observed as compared to UV LEDs with flat sapphire substrate. For UV LEDs with flat sapphire substrate [Figs. 4(a) and 4(d)], the TE-polarized light intensity is primarily concentrated at the center region. Despite the use of bottom-side PSS could redirect the light radiation pattern [Figs. 4(b)–4(c) and 4(e)–4(f)], it scatters more TE-polarized photons back into the LED structure than extracting them out through the sapphire substrate. To be more specific, as D increases from 180 nm to 280 nm, the TE-polarized $\eta_{extraction}$ drops from ~0.9-times and ~0.8-times for 230 nm and 280 nm

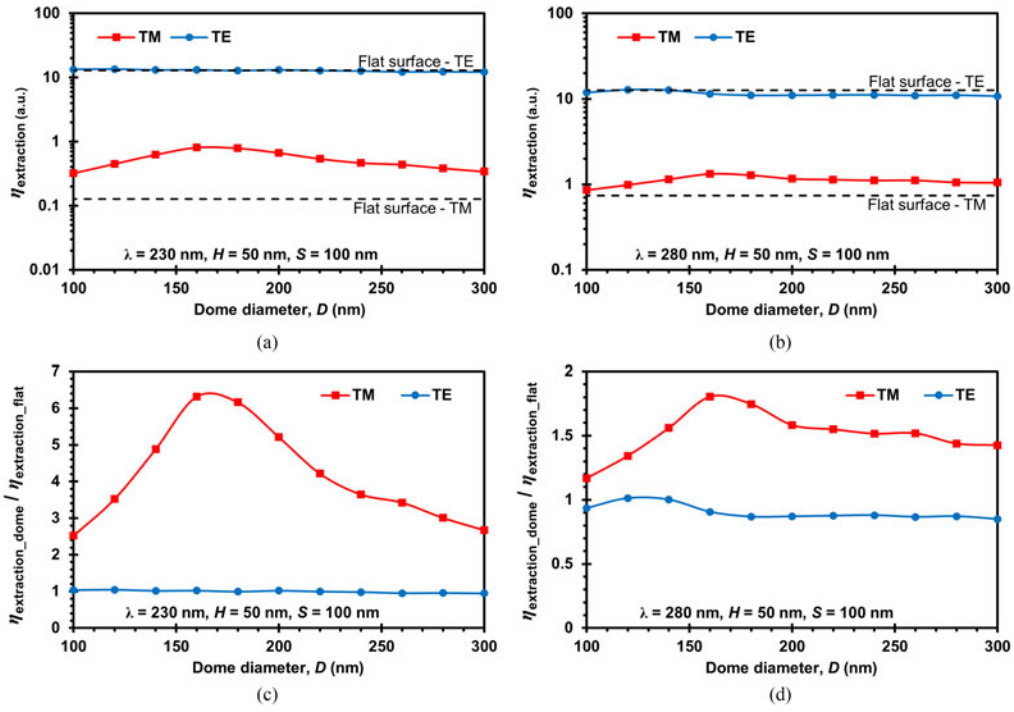

Fig. 5. The $\eta_{extraction}$ for AlGaN-based flip-chip UV LEDs with top side PSS at (a) $\lambda = 230$ nm and (b) $\lambda = 280$ nm as a function of D. The $\eta_{extraction}$ for UV LEDs with flat sapphire substrate are represented by the black dashed lines. Ratio of the $\eta_{extraction}$ for UV LEDs with top-side PSS ($\eta_{extraction\_dome}$) to the $\eta_{extraction}$ for UV LEDs with flat sapphire substrate ($\eta_{extraction\_flat}$) for (c) $\lambda = 230$ nm and (d) $\lambda = 280$ nm as a function of D.

UV LEDs respectively to ~0.8-times and ~0.7-times for 230 nm and 280 nm UV LEDs respectively. This degraded TE-polarized $\eta_{extraction}$ is also supported by the lower radiation intensity distributions observed in Figs. 4(b)–4(c) and 4(e)–4(f).

3.3 Flip-Chip UV LEDs With Microdome-Shaped Patterning on Top Surface of Sapphire Substrate

The enhancement of $\eta_{extraction}$ for flip-chip UV LEDs with top-side microdome-shaped PSS has been investigated here to understand the influence of microdome patterning to the mid- and deep-UV LED $\eta_{extraction}$. From the results presented in Fig. 5, TE-polarized $\eta_{extraction}$ are consistently higher than TM-polarized $\eta_{extraction}$ (>1 order of magnitude) for both 230 nm and 280 nm UV LEDs with top-side PSS. Nevertheless, significant enhancement in TM-polarized $\eta_{extraction}$ (up to ~6.3-times and ~1.8-times for 230 nm and 280 nm UV LEDs respectively) is observed as compared to TE-polarized $\eta_{extraction}$ (<5% enhancement for both 230 nm and 280 nm UV LEDs). As previously stated, TM-polarized light primarily travels at large angles with respect to c-axis while TE-polarized light mostly travels along c-axis, the curvature surface of the microdomes on sapphire substrate have more effects on extracting TM-polarized photons out of the LED structure than the TE-polarized photons. Comparable to the UV LEDs with bottom-side PSS, the UV LEDs with top-side PSS demonstrate strong dependence on D for TM-polarized $\eta_{extraction}$ but has negligible effect on TE-polarized $\eta_{extraction}$. Again, this is attributed to the function of the PSS that acts as an extractor for TM-polarized output and as a reflector for TE-polarized output (more details in the supporting information). As presented in Figs. 5(c) and 5(d), ~2.5-times to ~6.3-times and ~1.1-times to ~1.8-times enhancement in TM-polarized $\eta_{extraction}$ for 230 nm and 280 nm UV LEDs with top-side PSS respectively can be obtained for D ranges between 100 nm and 300 nm. Conversely, the ratio of TE-polarized $\eta_{extraction}$ for UV LEDs with top-side PSS to UV LEDs with flat sapphire substrate drops

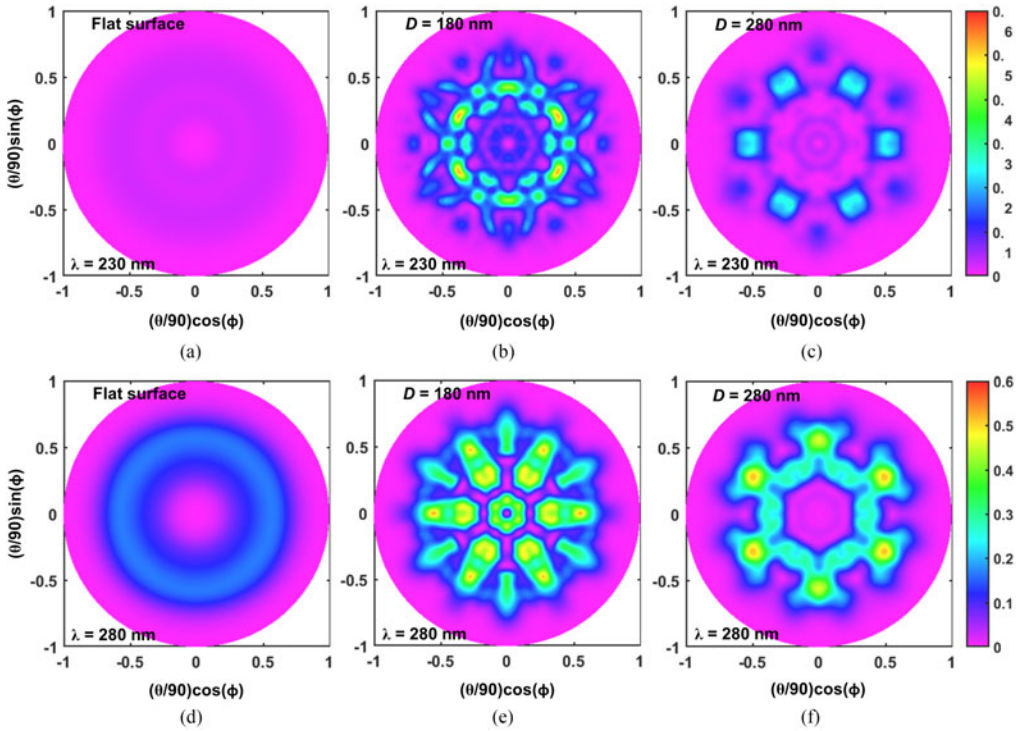

Fig. 6. TM-polarization far-field radiation patterns of 230 nm [(a)–(c)] and 280 nm [(d)–(f)] flip-chip UV LEDs with flat sapphire substrate [(a) & (d)], top-side PSS with $D = 180$ nm [(b) & (e)] and top-side PSS with $D = 280$ nm [(c) & (f)].

from ~1.04-times to ~0.95-times for 230 nm and ~1.01-times to ~0.85-times for 280 nm when D changes from 100 nm to 300 nm.

Similar with the case of bottom-side PSS, the microdome-shaped array patterning on the top-side of sapphire substrate also acts as a strong photons scattering center, which will impact the light extraction for the LED devices. From the far-field radiation patterns shown in Fig. 6, significantly higher radiant intensity can be observed for both 230 nm and 280 nm UV LEDs with top-side PSS at angle between ~10° and ~50° while the conventional UV LEDs with flat sapphire substrate exhibit symmetric donut-shaped radiation patterns with peak intensity at ~30°. This is primarily attributed to the curvature surfaces of the microdomes that result in larger photon escape cone than the conventional UV LEDs. Consequently, this spread-out distribution of high intensity radiation pattern leads to higher TM-polarized $\eta_{extraction}$ (up to ~6.3-times and 1.8-times for 230 nm and 280 nm respectively) as compared to the conventional UV LEDs with flat sapphire substrate.

For TE-polarization, employing the top-side PSS for both the 230 nm and 280 nm UV LEDs has very similar effect as those with bottom-side PSS. From the far-field radiation plots presented in Fig. 7, it is obvious that the top-side PSS for both the 230 nm and 280 nm UV LEDs are not a good extractor to enable TE-polarized photons to escape out of the LED structure through the sapphire substrate. Even though the top-side PSS acts as a strong scattering center and results in altered radiation patterns as compared to conventional UV LEDs with flat sapphire substrate, the fraction of TE-polarized photons that could be escaped out of the structure is not high enough to compensate for the fraction of photons being reflected back into the structure. In addition, despite higher radiation intensity can be observed at some regions of the far-field radiation plots presented in Fig. 7, particularly when $D = 280$ nm for 230 nm UV LEDs [Fig. 7(c)], majority of the area still observed extremely low radiation intensity (dark blue and purple region). Consequently, lower TE-polarized $\eta_{extraction}$ for the UV LEDs with top-side PSS as compared to UV LEDs with flat sapphire substrate has been resulted.

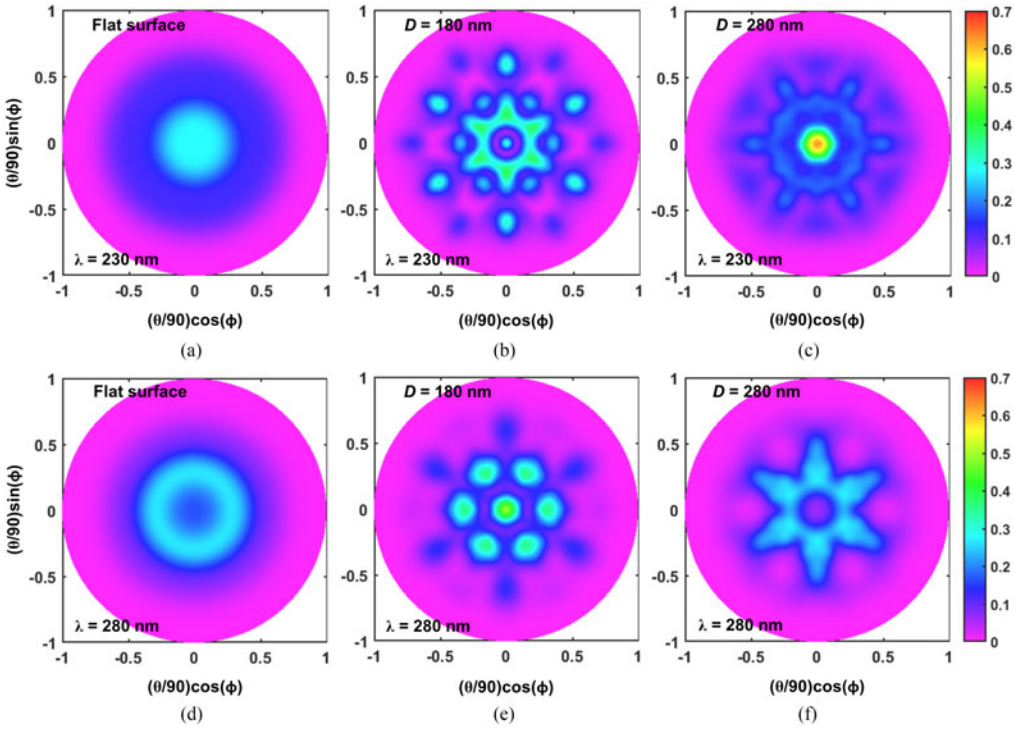

Fig. 7. TE-polarization far-field radiation patterns of 230 nm [(a)–(c)] and 280 nm [(d)–(f)] flip-chip UV LEDs with flat sapphire substrate [(a) & (d)], top-side PSS with $D = 180$ nm [(b) & (e)] and top-side PSS with $D = 280$ nm [(c) & (f)].

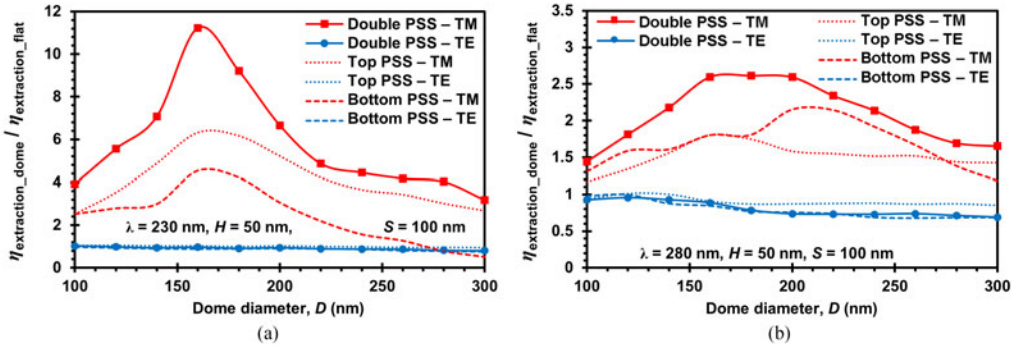

Fig. 8. Ratio of the $\eta_{extraction}$ for flip-chip UV LEDs with double-sided PSS ($\eta_{extraction\_dome}$) to the $\eta_{extraction}$ for flip-chip UV LEDs with flat sapphire substrate ($\eta_{extraction\_flat}$) for (a) $\lambda = 230$ nm and (b) $\lambda = 280$ nm as a function of D. The $\eta_{extraction}$ for flip-chip UV LEDs with top-side and bottom-side PSS are represented by the dotted lines and dashed lines respectively.

3.4 Flip-Chip UV LEDs With Microdome-Shaped Patterning on Both Sides of Sapphire Substrate

The results for both 230 nm and 280 nm flip-chip UV LEDs with single-sided (bottom-side or top-side) microdome-shaped PSS in previous sub-sections have demonstrated significant enhancement for TM-polarized $\eta_{extraction}$ but degraded TE-polarized $\eta_{extraction}$ when D changes from 100 nm to 300 nm. Here, we examine the effect of combining the bottom-side and top-side patterning on the TE- and TM-polarized $\eta_{extraction}$ for both 230 nm and 280 nm flip-chip UV LEDs. The enhancement ratio for the UV LEDs with double-sided patterning normalized to conventional UV LEDs with flat sapphire substrate are presented in Fig. 8(a) for $\lambda = 230$ nm and Fig. 8(b) for $\lambda = 280$ nm. The $\eta_{extraction}$ ratio

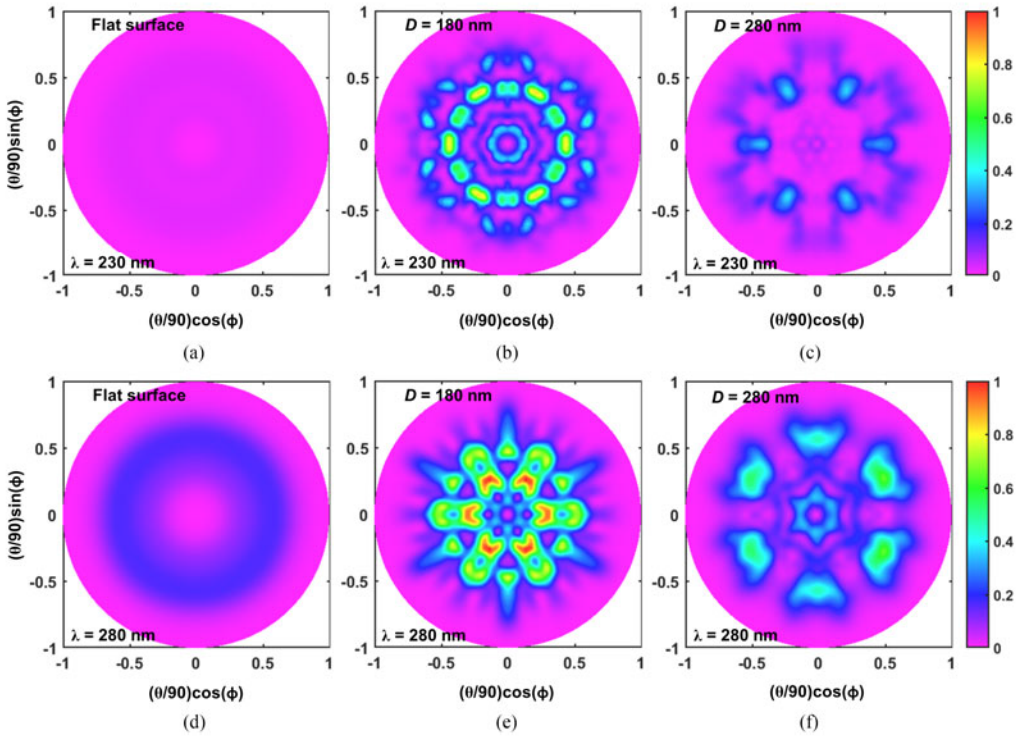

Fig. 9. TM-polarization far-field radiation patterns of 230 nm [(a)–(c)] and 280 nm [(d)–(f)] flip-chip UV LEDs with flat sapphire substrate [(a) & (d)], double-sided PSS with $D = 180$ nm [(b) & (e)] and double-sided PSS with $D = 280$ nm [(c) & (f)].

for UV LEDs with top-side and bottom-side PSS represented by dotted lines and dashed lines respectively are also plotted in Fig. 8 for comparison.

From the results presented in Fig. 8, the use of double-sided PSS will result in even higher TM-polarized $\eta_{extraction}$ than the single-sided PSS where up to ~11.2-times and ~2.6-times enhancement can be obtained for 230 nm and 280 nm UV LEDs respectively as compared to UV LEDs with flat sapphire substrate. These substantial improvements for TM-polarized $\eta_{extraction}$ by employing double-sided PSS are attributed to the strong light scattering effects coming from both the top-side and bottom-side patterning, which is evidenced in the cross-sectional near-field electric field intensity plots presented in Figs. S1 & S2 in the supplementary information. In particular, the TM-polarized $\eta_{extraction}$ for the double-sided PSS are very similar to as taking the superposition of the TM-polarized $\eta_{extraction}$ for the bottom-side and top-side patterning. Nevertheless, the enhancement ratio is not exactly the same as by adding the TM-polarized $\eta_{extraction}$ from the bottom-side and top-side patterning due to the destructive interference. For 230 nm UV LEDs with double-sided PSS, the peak TM-polarized $\eta_{extraction}$ enhancement occurs at $D = 160$ nm, which is the same as those with bottom-side or top-side PSS [Fig. 8(a)]. However, for the case of 280 nm UV LEDs, as the peak TM-polarized $\eta_{extraction}$ enhancement for bottom-side and top-side PSS occurs at different D (200 nm for bottom-side PSS and 160 nm for top-side PSS), a broad TM-polarized $\eta_{extraction}$ enhancement ratio peak for double-sided PSS has been observed [Fig. 8(b)]. Specifically, the TM-polarized $\eta_{extraction}$ enhancement ratio for 280 nm UV LEDs with double-sided PSS are approximately ~2.6-times for D ranges between 160 nm and 200 nm.

In order to prove that the significantly enhanced TM-polarized $\eta_{extraction}$ for the UV LEDs with double-sided PSS are resulted from the superposition of the bottom-side and top-side patterning, the TM-polarized far-field radiation patterns for UV LEDs with double-sided PSS have been plotted in Fig. 9. Figs. 9(a)–9(c) are the TM-polarized far-field radiation patterns for 230 nm UV LEDs and Figs. 9(d)–(f) show the far-field emission patterns for 280 nm UV LEDs. By comparing the

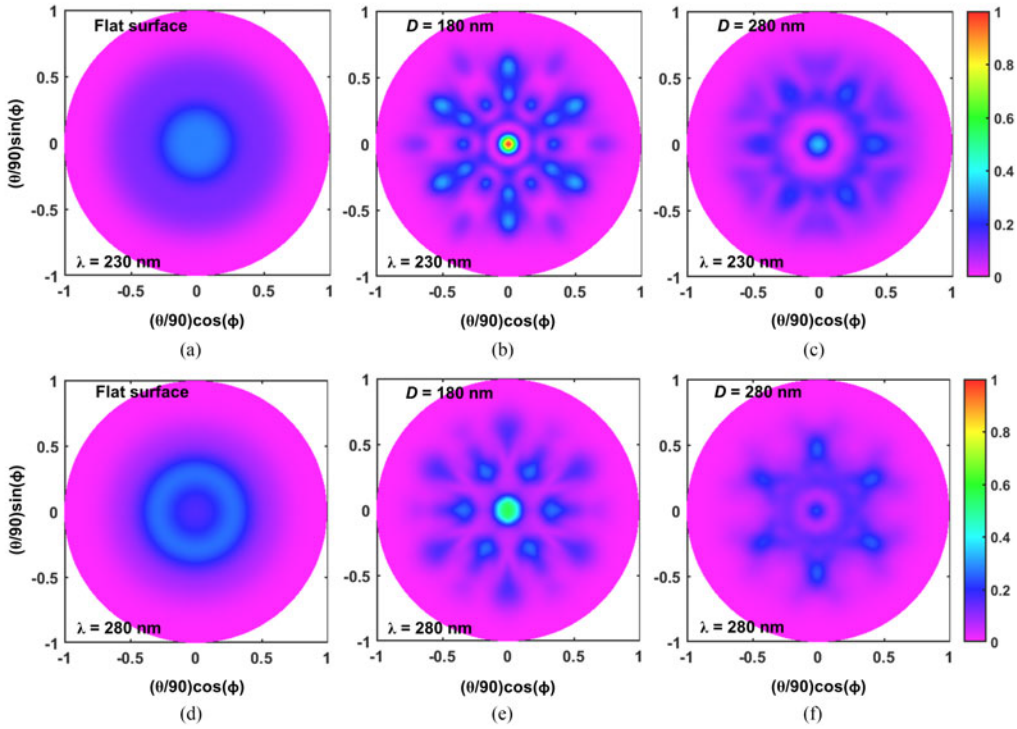

Fig. 10. TE-polarization far-field radiation patterns of 230 nm [(a)–(c)] and 280 nm [(d)–(f)] flip-chip UV LEDs with flat sapphire substrate [(a) & (d)], double-sided PSS with $D = 180$ nm [(b) & (e)] and double-sided PSS with $D = 280$ nm [(c) & (f)].

TM-polarized far-field radiation plots for the UV LEDs with double-sided PSS [Fig. 9] to those with bottom-side PSS [Fig. 3] and top-side PSS [Fig. 6], it is obvious that the radiation patterns for double-sided patterning are basically the combination of the far-field radiation patterns from the top-side and bottom-side patterning. As an example, for the case of $D = 180$ nm for 230 nm UV LEDs, the UV LED with bottom-side PSS has emission patterns at angle ranges from ~25° to ~40° [Fig. 3(b)] while the UV LED with top-side PSS has emission patterns at angle ranges from ~10° to ~50° [Fig. 6(b)]. From Fig. 9(b), it is obvious that the 230 nm UV LEDs with double-sided PSS has very similar emission patterns as those with bottom-side patterning and top-side patterning at angles between ~10° to ~50°. In particular, large radiation intensity can be observed at angles between ~25° and ~40°.

On the contrary, the use of double-sided PSS for both 230 nm and 280 nm flip-chip UV LEDs does not lead to enhanced TE-polarized $\eta_{extraction}$ when D ranges between 100 nm and 300 nm (blue solid lines in Fig. 8), which is similar to the phenomena observed for the case of flip-chip UV LEDs with bottom-side PSS and top-side PSS (blue dashed lines and dotted lines in Fig. 8). This has been expected as the single-sided PSS has been observed to primarily act as reflector to prevent TE-polarized photons extraction through the sapphire substrate. As a result, smaller TE-polarized $\eta_{extraction}$ has been obtained as compared to UV LEDs with flat sapphire substrate. In addition, the TE-polarized $\eta_{extraction}$ for UV LEDs with double-sided PSS are primarily limited by the bottom-side patterning as the bottom reflector only allow very minimum amount of TE-polarized photons to pass through. As can been seen from the TE-polarized far-field radiation patterns plotted in Fig. 10, the emission patterns for TE-polarized 230 nm and 280 nm UV LEDs with double-sided PSS are primarily the combination radiation patterns of those with bottom-side patterning (Fig. 4) and top-side patterning (Fig. 7). For instance, for the case of $D = 280$ nm for 280 nm UV LEDs, the UV LEDs with bottom-side PSS exhibit circular-shaped far-field emission pattern [Fig. 4(f)] while the UV LEDs with top-side PSS has a star-shaped like far-field emission pattern [Fig. 7(f)].

4. Conclusion

The TE- and TM-polarized $\eta_{extraction}$ for 230 nm and 280 nm flip-chip UV LEDs with microdome-shaped array patterning on sapphire substrate have been investigated. In particular, the TE- and TM-polarized $\eta_{extraction}$ for UV LEDs with bottom-side patterning, top-side patterning, and double-sided patterning have been studied and compared. Our analysis shows that the microdome-shaped PSS with $H = 50$ nm, $S = 100$ nm, and $D = 100$–300 nm are particularly efficient in enhancing TM-polarized $\eta_{extraction}$ where up to ~4.5-times and ~2.2-times can be obtained for 230 nm and 280 nm flip-chip UV LEDs with bottom-side PSS respectively, and ~6.3-times and ~1.8-times for 230 nm and 280 nm flip-chip UV LEDs with top-side PSS respectively. The significant improvement obtained in the TM-polarized $\eta_{extraction}$ is attributed to the enhanced scattering effect introduced by the microdome-shaped array that enable the TM-polarized photons to escape out of the structure. As a result, the use of double-sided PSS could result in even higher TM-polarized $\eta_{extraction}$ where up to ~11.2-times and ~2.6-times improvement can be achieved for 230 nm and 280 nm flip-chip UV LEDs respectively. For both emission wavelengths, the peak TM-polarized $\eta_{extraction}$ is observed when D is ~70–100 nm below the emission wavelength. Accordingly, higher η_{EQE} from UV LEDs employing PSS is expected as a result of dominant TM-polarized spontaneous emission and larger TM-polarized $\eta_{extraction}$. On the contrary, the use of single-sided PSS does not lead to enhanced TE-polarized $\eta_{extraction}$ for both the 230 nm and 280 nm flip-chip UV LEDs. The PSS is actually acting as a reflector that reflect majority of the TE-polarized light back into the structure. Consequently, lower TE-polarized $\eta_{extraction}$ for flip-chip UV LEDs with single-sided PSS as compared to flip-chip UV LEDs with flat sapphire substrate are resulted. It is expected that this study will shed light on the design of flip-chip UV LEDs with microstructure PSS for both mid- and deep-UV regimes to achieve high-efficiency AlGaN-based UV LEDs.

References

[1] H. Hirayama, S. Fujikawa, and N. Kamata, "Recent progress in AlGaN-based deep-UV LEDs," *Electron. Commun. Jpn.*, vol. 98, no. 5, pp. 1–8, May 2015.

[2] Y. Muramoto, M. Kimura, and S. Nouda, "Development and future of ultraviolet light-emitting diodes: UV-LED will replace the UV lamp," *Semicond. Sci. Technol.*, vol. 29, no. 8, Jun. 2014, Art. no. 84004.

[3] M. Kneissl *et al.*, "Advances in group III-nitride-based deep UV light-emitting diode technology," *Semicond. Sci. Technol.*, vol. 26, no. 1, Jan. 2011, Art. no. 14036.

[4] M. S. Shur and R. Gaska, "Deep-ultraviolet light-emitting diodes," *IEEE Trans. Electron Devices*, vol. 57, no. 1, pp. 12–25, Jan. 2010.

[5] Y. Zhang *et al.*, "Interband tunneling for hole injection in III-nitride ultraviolet emitters," *Appl. Phys. Lett.*, vol. 106, no. 14, p. 141103, Apr. 2015.

[6] F. Mehnke *et al.*, "Efficient charge carrier injection into sub-250 nm AlGaN multiple quantum well light emitting diodes," *Appl. Phys. Lett.*, vol. 105, no. 5, p. 51113, Aug. 2014.

[7] B. H. Le, S. Zhao, X. Liu, S. Y. Woo, G. A. Botton, and Z. Mi, "Controlled coalescence of AlGaN nanowire arrays: An architecture for nearly dislocation-free planar ultraviolet photonic device applications," *Adv. Mater.*, vol. 28, no. 38, pp. 8446–8454, Oct. 2016.

[8] K. Ban *et al.*, "Internal quantum efficiency of whole-composition-range AlGaN multiquantum wells," *Appl. Phys. Exp.*, vol. 4, no. 5, p. 52101, Apr. 2011.

[9] J. Zhang, H. Zhao, and N. Tansu, "Effect of crystal-field split-off hole and heavy-hole bands crossover on gain characteristics of high Al-content AlGaN quantum well lasers," *Appl. Phys. Lett.*, vol. 97, no. 11, p. 111105, Sep. 2010.

[10] J. E. Northrup *et al.*, "Effect of strain and barrier composition on the polarization of light emission from AlGaN/AlN quantum wells," *Appl. Phys. Lett.*, vol. 100, no. 2, p. 21101, Jan. 2012.

[11] Y. Chang, F. Chen, S. Li, and Y. Kuo, "Electrical polarization effects on the optical polarization properties of AlGaN ultraviolet light-emitting diodes," *IEEE Trans. Electron Devices*, vol. 61, no. 9, pp. 3233–3238, Sep. 2014.

[12] Z. Bryan, I. Bryan, S. Mita, J. Tweedie, Z. Sitar, and R. Collazo, "Strain dependence on polarization properties of AlGaN and AlGaN-based ultraviolet lasers grown on AlN substrates," *Appl. Phys. Lett.*, vol. 106, no. 23, p. 232101, Jun. 2015.

[13] M. Shatalov *et al.*, "AlGaN deep-ultraviolet light-emitting diodes with external quantum efficiency above 10%," *Appl. Phys. Exp.*, vol. 5, no. 8, p. 82101, Jul. 2012.

[14] T. Takano, T. Mino, J. Sakai, N. Noguchi, K. Tsubaki, and H. Hirayama, "Deep-ultraviolet light-emitting diodes with external quantum efficiency higher than 20% at 275 nm achieved by improving light-extraction efficiency," *Appl. Phys. Exp.*, vol. 10, no. 3, p. 31002, Mar. 2017.

[15] S. A. Nikishin *et al.*, "Deep ultraviolet light emitting diodes based on short period superlattices of AlN/AlGa(In)N," *Jpn. J. Appl. Phys.*, vol. 42, no. Part 2, No. 11B, pp. L1362–L1365, Nov. 2003.

[16] C. Pernot *et al.*, "Improved efficiency of 255–280 nm AlGaN-based light-emitting diodes," *Appl. Phys. Exp.*, vol. 3, no. 6, p. 61004, Jun. 2010.

[17] H. Hirayama, N. Noguchi, and N. Kamata, "222 nm deep-ultraviolet AlGaN quantum well light-emitting diode with vertical emission properties," *Appl. Phys. Exp.*, vol. 3, no. 3, p. 32102, Mar. 2010.
[18] Y. Liao, C. Thomidis, C. Kao, and T. D. Moustakas, "AlGaN based deep ultraviolet light emitting diodes with high internal quantum efficiency grown by molecular beam epitaxy," *Appl. Phys. Lett.*, vol. 98, no. 8, p. 81110, Feb. 2011.
[19] T. Kinoshita *et al.*, "Performance and reliability of deep-ultraviolet light-emitting diodes fabricated on AlN substrates prepared by hydride vapor phase epitaxy," *Appl. Phys. Exp.*, vol. 6, no. 9, p. 92103, Sep. 2013.
[20] P. Dong *et al.*, "282 nm AlGaN-based deep ultraviolet light-emitting diodes with improved performance on nano-patterned sapphire substrates," *Appl. Phys. Lett.*, vol. 102, no. 24, p. 241113, Jun. 2013.
[21] N. Maeda and H. Hirayama, "Realization of high-efficiency deep-UV LEDs using transparent p-AlGaN contact layer," *Phys. Status Solidi*, vol. 10, no. 11, pp. 1521–1524, Nov. 2013.
[22] E. Francesco Pecora *et al.*, "Sub-250 nm light emission and optical gain in AlGaN materials," *J. Appl. Phys.*, vol. 113, no. 1, p. 13106, Jan. 2013.
[23] J. J. Wierer, A. A. Allerman, I. Montaño, and M. W. Moseley, "Influence of optical polarization on the improvement of light extraction efficiency from reflective scattering structures in AlGaN ultraviolet light-emitting diodes," *Appl. Phys. Lett.*, vol. 105, no. 6, p. 61106, Aug. 2014.
[24] D. Y. Kim *et al.*, "Overcoming the fundamental light-extraction efficiency limitations of deep ultraviolet light-emitting diodes by utilizing transverse-magnetic-dominant emission," *Light Sci. Appl.*, vol. 4, no. 4, Apr. 2015, Art. no. e263.
[25] C. Liu, Y. K. Ooi, and J. Zhang, "Proposal and physics of AlInN-delta-GaN quantum well ultraviolet lasers," *J. Appl. Phys.*, vol. 119, no. 8, p. 83102, Feb. 2016.
[26] S. Islam, V. Protasenko, S. Rouvimov, H. G. Xing, and D. Jena, "Sub-230 nm deep-UV emission from GaN quantum disks in AlN grown by a modified Stranski–Krastanov mode," *Jpn. J. Appl. Phys.*, vol. 55, no. 5S, p. 05FF06, May 2016.
[27] C. Liu *et al.*, "Physics and polarization characteristics of 298 nm AlN-delta-GaN quantum well ultraviolet light-emitting diodes," *Appl. Phys. Lett.*, vol. 110, no. 7, p. 71103, Feb. 2017.
[28] M. Lapeyrade *et al.*, "Design considerations for AlGaN-based UV LEDs emitting near 235 nm with uniform emission pattern," *Semicond. Sci. Technol.*, vol. 32, no. 4, pp. 045019/1–045019/8, Apr. 2017.
[29] C. Liu, Y. K. Ooi, S. M. Islam, H. G. Xing, D. Jena, and J. Zhang, "234 nm and 246 nm AlN-Delta-GaN quantum well deep ultraviolet light-emitting diodes," *Appl. Phys. Lett.*, vol. 112, no. 1, p. 11101, Jan. 2018.
[30] H.-Y. Ryu, I.-G. Choi, H.-S. Choi, and J.-I. Shim, "Investigation of light extraction efficiency in AlGaN deep-ultraviolet light-emitting diodes," *Appl. Phys. Exp.*, vol. 6, no. 6, p. 62101, Jun. 2013.
[31] K. H. Lee *et al.*, "Light-extraction efficiency control in AlGaN-based deep-ultraviolet flip-chip light-emitting diodes: A comparison to InGaN-based visible flip-chip light-emitting diodes," *Opt. Exp.*, vol. 23, no. 16, p. 20340, Aug. 2015.
[32] M. Kim *et al.*, "AlGaN-based deep ultraviolet light-emitting diodes fabricated on patterned sapphire substrates," *Appl. Phys. Exp.*, vol. 4, no. 9, p. 92102, Aug. 2011.
[33] P. Zhao, L. Han, M. R. McGoogan, and H. Zhao, "Analysis of TM mode light extraction efficiency enhancement for deep ultraviolet AlGaN quantum wells light-emitting diodes with III-nitride micro-domes," *Opt. Mater. Exp.*, vol. 2, no. 10, p. 1397, Oct. 2012.
[34] Y. K. Ooi, C. Liu, and J. Zhang, "Analysis of polarization-dependent light extraction and effect of passivation layer for 230 nm AlGaN nanowire light-emitting diodes," *IEEE Photon. J.*, vol. 9, no. 4, Aug. 2017, Art. no. 4501712.
[35] M. Djavid and Z. Mi, "Enhancing the light extraction efficiency of AlGaN deep ultraviolet light emitting diodes by using nanowire structures," *Appl. Phys. Lett.*, vol. 108, no. 5, p. 51102, Feb. 2016.
[36] H.-Y. Ryu, "Large enhancement of light extraction efficiency in AlGaN-based nanorod ultraviolet light-emitting diode structures," *Nanoscale Res. Lett.*, vol. 9, no. 1, p. 58, 2014.
[37] Synopsys's Optical Solutions Group, Pasadena, CA, USA. *FullWAVE*. [Online]. Available: https://optics.synopsys.com
[38] P. Zhu, G. Liu, J. Zhang, and N. Tansu, "FDTD analysis on extraction efficiency of GaN light-emitting diodes with microsphere arrays," *J. Disploay Technol.*, vol. 9, no. 5, pp. 317–323, May 2013.
[39] E. D. Palik, *Handbook Optical Constants Solids. San Francisco, CA, USA*: Academic, 1998.
[40] C. H. Yan, H. Yao, J. M. Van Hove, A. M. Wowchak, P. P. Chow, and J. M. Zavada, "Ordinary optical dielectric functions of anisotropic hexagonal GaN film determined by variable angle spectroscopic ellipsometry," *J. Appl. Phys.*, vol. 88, no. 6, pp. 3463–3469, Sep. 2000.
[41] H. Hirayama *et al.*, "222–282 nm AlGaN and InAlGaN-based deep-UV LEDs fabricated on high-quality AlN on sapphire," *Phys. Status Solidi*, vol. 206, no. 6, pp. 1176–1182, Jun. 2009.
[42] P. Zhu, "Frustrated total internal reflection in organic light-emitting diodes employing sphere cavity embedded in polystyrene," *J. Opt.*, vol. 18, no. 2, p. 25403, Feb. 2016.